scientific reports

Check for updates

OPEN

# Obinutuzumab induces lysosomal destabilization via sphingomyelin-dependent inhibition of TRPML2

Jinkyung Oh[1], Narae Jin[1], Sunhyung Kwon[1], Changsin Lee[1], Hyungjun Baek[1], Donghyuk Lee[1,2] & Joo Young Kim[1,2]✉

**Obinutuzumab (OBI), a type II glycoengineered anti-CD20 antibody, induces direct cell death (DCD) in B-cell lymphomas more effectively than rituximab, yet the upstream mechanisms underlying this activity remain unclear. Here, we identify a lipid–ion channel axis linking antibody internalization to lysosomal destabilization. Using imaging, genetic, and biochemical approaches, we show that OBI is rapidly internalized into acidic compartments where it colocalizes with sphingomyelin (SM). SM-dependent inhibition of TRPML2-mediated lysosomal $Ca^{2+}$ release sensitizes lysosomes to OBI-induced stress, lowering the threshold for LMP and direct cell death. Restoration of TRPML2 function by SMase treatment, or blockade of OBI internalization, attenuates LMP and DCD, underscoring the critical role of the SM–TRPML2 pathway. These findings reveal a previously uncharacterized mechanism by which OBI exerts cytotoxicity, highlighting lipid remodeling and ion channel regulation as potential targets to enhance the efficacy of antibody-based therapies in B-cell malignancies.**

**Keywords** Obinutuzumab, TRPML2, Lysosomal membrane permeabilization, Sphingomyelin, Endocytosis, B-cell lymphoma

**Abbreviations**

| | |
|---|---|
| ADCC | Antibody-dependent cellular cytotoxicity |
| CDC | Complement-dependent cytotoxicity |
| DCD | Direct cell death |
| DAR | Dye-to-antibody ratio |
| LMP | Lysosome membrane permeabilization |
| LT | Lysotracker |
| OBI | Obinutuzumab |
| OGB-d | Oregon Green BAPTA-1 Dextran |
| RTX | Rituximab |
| SM | Sphingomyelin |
| SMase | Sphingomyelinase |
| TRPML | Transient receptor potential mucolipin |
| PI | Propidium iodide |

B-cell malignancies, including various subtypes of lymphomas, remain a major clinical challenge despite advancements in targeted immunotherapy. Anti-CD20 monoclonal antibodies (mAbs) such as rituximab (RTX) have significantly improved B-cell lymphoma treatment by inducing cytotoxicity through multiple mechanisms, including antibody-dependent cellular cytotoxicity (ADCC), complement-dependent cytotoxicity (CDC), and direct cell death (DCD)[1,2]. Among these, obinutuzumab (OBI), a glycoengineered type II anti-CD20 mAb, has demonstrated superior efficacy over RTX, primarily through DCD, which results from antigen binding rather than Fc-mediated immune effector functions[3,4]. This mechanism contributes to OBI's therapeutic advantages, including reduced resistance, minimized residual disease, and prolonged progression-free survival[5–7].

A hallmark of OBI-induced DCD is lysosomal membrane permeabilization (LMP), which results in the release of hydrolytic enzymes such as cathepsins and activation of lysosome-dependent cell death pathways[8–11]. In leukocytes, LMP acts as an early driver of apoptosis by enabling cathepsin-dependent Bid cleavage and downstream mitochondrial damage, highlighting its causal role in immune-cell death pathways[12]. While the

[1]Department of Pharmacology and Brain, Korea 21 Project for Medical Science, Yonsei University College of Medicine, 50-1 Yonsei-Ro, Seodaemun-Gu, Seoul 03080, Republic of Korea. [2]Woo Choo Lee Institute for Precision Drug Development, Seoul, Republic of Korea. ✉email: jooyoungkim@yuhs.ac

downstream effects of LMP, such as cathepsin-mediated cytotoxicity, are well characterized[13], the upstream molecular mechanisms that render lysosomes susceptible to OBI-induced destabilization remain poorly understood. Lysosomal integrity is maintained by a balance of factors including lipid composition, fission–fusion dynamics, ion transport, and membrane trafficking[10,14]. Perturbations in these processes can prime lysosome membrane permeabilization all of which may prime lysosomes membrane permeabilization and cell death.

Recent evidence suggests that lysosomal volume regulation influences cellular sensitivity to LMP[15,16] Hypotonic conditions, which promote lysosomal swelling, enhance OBI-induced LMP, whereas hypertonic conditions, which reduce lysosomal volume, mitigate this effect. Osmotic stress in lysosomes is relieved by multiple ion channels in lysosomes. Among lysosomal ion channels, transient receptor potential mucolipins (TRPMLs) play central roles in maintaining lysosomal stability. TRPML1 mediates lysosomal fusion and fission, and its loss of function has been linked to impaired acidification, cathepsin B release, and lysosome-dependent cell death[17–20]. TRPML2, in turn, functions as an osmo- and mechanosensitive $Ca^{2+}$ channel, releasing lysosomal $Ca^{2+}$ in response to changes in membrane tension and osmotic stress[21–23]. Given these properties, we reasoned that TRPML2 activity could contribute to maintaining lysosomal integrity during the endocytic and biophysical stress imposed by OBI. We therefore hypothesized that pharmacological inhibition of TRPML channels would exacerbate OBI-induced LMP and DCD.

Notably, sphingomyelin (SM), a lipid highly enriched in plasma membranes, is a known inhibitor of TRPML channels and has been implicated in lysosomal dysfunction[24]. Therefore, we further considered whether OBI-induced lysosomal destabilization may involve lipid-mediated inhibition of TRPML channels, particularly via SM accumulation.

In this study, we aimed to elucidate the molecular mechanisms underlying OBI-induced LMP and DCD by investigating the role of lysosomal ion dynamics. Our findings suggest that OBI-mediated endocytosis facilitates the accumulation of SM within lysosomal membranes, which in turn suppresses TRPML2 function and promotes LMP. Understanding this pathway may offer new therapeutic strategies for enhancing anti-CD20 monoclonal antibody efficacy in B-cell lymphoma.

## Materials and methods

### Cell lines

Raji B cells were gifted by Prof. Seong Hwan Kim at Chungnam National University. Ramos cells and HeLa cells were purchased from Korean Cell Line Bank. Cells were maintained in RPMI-1640 or DMEM medium supplemented with 10% FBS and 1% penicillin–streptomycin at 37 °C in 5% $CO_2$ incubator. For expressing CD20/DsRED and GCamp-TRPML2 in HeLa cells, Lipofectomine 2000 reagent was used. Generation of GCaMP6s–TRPML constructs. All TRPML1 and TRPML2 constructs were generated using human-origin TRPML1/2 genes. The GCaMP6s–TRPML1 and GCaMP6s–TRPML2 coding sequences were subcloned into the lentiviral backbone pLenti6P for expression experiments. The $TRPML2^{Va}$ variant was generated by site-directed mutagenesis and subsequently cloned into pLenti6P in the same manner.

### Construction of sgRNA/siRNA knockdown cell lines targeting TRPML1 and TRPML2

Raji B cells were lentivirally transduced with SFFV-dCas9-mCherry-KRAB (Addgene #180264) to generate CRISPRi Raji B cell lines. To establish TRPML knockdown lines, dCas9-expressing Raji B cells were further transduced with sgRNAs targeting TRPML1 or TRPML2, as well as a control sgRNA, and selected with 1 μg/mL puromycin (ant-pr-1, Invivogen). For knockdown validation, total RNA was extracted from $5 \times 10^6$ Raji B cells using TRIzol reagent, and RT-qPCR was performed to measure TRPML1 and TRPML2 expression, normalized to GAPDH. TRPML 1–2 and TRPML 2–2 cell lines, which showed the most efficient knockdown, were selected for subsequent experiments. The sequences used were as follows: sgTRPML1_1 (forward, 5′-TTG GAC AGA TCA GCT GAT GCC GGA GTT TAA GAG C-3′; reverse, 5′-TTA GCT CTT AAA CTC CGG CAT CAG CTG ATC TGT CCA ACA AG-3′), sgTRPML2_1 (forward, 5′-TTG GGC AGA CCC CGG CCC GAG AGC GTT TAA GAG C-3′; reverse, 5′-TTA GCT CTT AAA CGC TCT CGG GCC GGG GTC TGC CCA ACA AG-3′), sgTRPML1_2 (forward, 5′-TTG GGA GCG AGG TCG CAG TGA CAG GTT TAA GAG C-3′; reverse, 5′-TTA GCT CTT AAA CCT GTC ACT GCG ACC TCG CTC CCA ACA AG-3′), and sgTRPML2_2 (forward, 5′-TTG GTG CGG CGG GCA GTT CTC GGG GTT TAA GAG C-3′; reverse, 5′-TTA GCT CTT AAA CCC CGA GAA CTG CCC GCC GCA CCA ACA AG-3′).

For siRNA transfection, $2 \times 10^4$ Raji cell were seed per 24-well in 500ul media. To prepare the transfection complexes, 2 μL of transfection reagent (Lipofectamine 3000, invitrogen) was diluted in 50 μL of OPTI-$MEM^R$ (Gibco) and incubated for 5 min at room temperature. Separately, 2 μL of siRNA solution (20 μM stock; equivalent to 40 pmol siRNA, Gencefe Biotech) was diluted in 50 μL of serum-free medium and incubated for 5 min. The diluted transfection reagent was then combined with the diluted siRNA solution, gently mixed, and incubated for an additional 20 min at room temperature to allow complex formation. A total of 100 μL of the transfection complex was subsequently added to each well, and the plate was gently agitated to ensure even distribution. After 16 h, the medium was replaced with complete growth medium. Cells were then incubated at 37 °C incubator for 24–72 h for analysis of mRNA expression via qPCR.

### Lysosomal membrane permeabilization and direct cell death assay

$5.0 \times 10^4$ Raji cells were seeded in a 96-well plate and treated with hypertonic (200 mM sucrose) and hypotonic (60% water) mediums for 2 h, followed by OBI (0.3 μg/ml) for 4 h. In addition, TRPML-targeting sgRNA- or siRNA-transfected cells were treated with OBI in a time-dependent manner. For drug treatments, (1R,2R)-ML-SI3 (HY-134819A; MCE), ML2-SA1 (axon Medchem), and 3-*O*-methyl Estradiol (#42995, Cayman Chemical) were administered for 2 h at 37 °C, followed by OBI (0.3 μg/ml) treatment for an additional 2 h. Endocytosis inhibition was performed using filipin (HY-N6716, MCE), dynasore (S8047, Sellekchem), pitstop2 (HY-

115605, MCE), Sphingomyelinase (S7651-10UN, Sigma), or heat-inactivated Sphingomyelinase for 30 min at 37 °C before antibodies treatment (10 μg/ml, IgG, RTX, OBI). All cells were stained with LysoTracker (L12492, Invitrogen) or PI (P4170-10 mg, Sigma) for 30 min and analyzed using a FACSymphony A5 (BD Biosciences). LMP was quantified as the percentage of cells that exhibited complete loss of LysoTracker Deep Red signal (LysoTracker-negative cells) compared with untreated controls. A cell was scored as LysoTracker-negative when its mean punctate LysoTracker intensity fell below a predefined threshold determined from the distribution of untreated control cells (background + SD). Cell death was quantified as the percentage of cells showing complete loss of calcein fluorescence (calcein-negative cells) using a threshold defined relative to untreated controls.

### Cathepsin B release measurement

To assess the release of cathepsin B, cells treated with each condition was harvested and subsequently fixed using BD Cytofix/Cytoperm™ Fixation/Permeabilization kit (BD Biosciences, #554714) at room temperature for 15 min, followed by a briefly rinse with wash buffer. Fixed cells were incubated overnight at 4 °C with a primary anti-cathepsin B antibody (ab58802, abcam). After two washes, an Alexa Fluor 647-conjugated anti-mouse secondary antibody (1:1000) was applied according to the manufacturer's protocol. Following three additional washes, cells were mounted using fluorescence mounting medium (S3023, Dako, Glostrup, Denmark) for immunofluorescence analysis. Alexa Fluor 647 fluorescence intensity was evaluated with a Zeiss LSM 700 confocal microscope.

### Lysosome vacuolization imaging

$5.0 \times 10^4$ Raji cells were seeded in a 96-well plate and treated with (1R, 2R)-ML-SI3, hypertonic, and hypotonic medium for 2 h. Cells were stained with 100 nM LT Deep Red for 30 min. Cells were centrifuged and resuspended in 4 μl fluorescent mounting media on a cover glass visualized under a Zeiss LSM 700 microscope. Vacuoles are shown as red spots.

### Measurement of lysosomal $Ca^{2+}$ release by Fluo-4

Single cell $[Ca^{2+}]_i$ imaging was measured by recording Fluo-4 (F14201, Invitrogen) at excitation wavelengths of 494 nm. $5 \times 10^4$ HeLa cells were plated in 18 mm round cover glass (Paul Marienfeld GmbH & Co. KG, Lauda-Königshofen, Germany). After expressing CD20/DsRED in HeLa cells by transfection, the cells were added with 1 μM Fluo-4 and incubated at 37℃ in an incubator enriched with 5% $CO_2$ atmosphere incubator for 30 min. And Fluo-4 fluorescence was measured with a confocal microscopy (LSM 710, Zeiss). Cells were treated with a solution containing 150 mM NaCl, 5 mM KCL, 1 mM $MgCl_2$, 1.5 mM $CaCl_2$, 10 mM glucose, 10 mM HEPES (pH 7.4 adjusted with NaOH). The osmolality of all solutions was adjusted to 310 osm with the major salt. The Fluo-4 fluorescence was recorded using wavelengths at 494 nm, and emission wavelengths above 506 nm were monitored. Cells were treated with indicated mAbs (10 μg/ml) and ML-SA1 (20 μM). And then, each single whole cell boundary was drawn and analyzed the intracellular $Ca^{2+}$ concentration during the experiments.

### Measurement of lysosomal $Ca^{2+}$ release by Oregon green BAPTA1-dextran

Ramos cells were stained with Oregon Green 488 BAPTA-1 dextran (O6798, Invitrogen) (100 μg/ml) at 37℃ in the culture medium for 12 h, and then washed for additional 10 h wash. During fluorescence measurements, the cells were continually in the 1.5 mM $Ca^{2+}$ regular solution containing 150 mM NaCl, 5 mM KCL, 1 mM $MgCl_2$, 10 mM glucose, 10 mM HEPES (pH 7.4 adjusted with NaOH). The osmolality of all solutions was adjusted to 310 osm with the major salt. Cells were treated with indicated mAbs (10 μg/ml) and ML-SA1 (20 μM). Change of fluorescence were presented as the change of the fluorescence intensity (ΔF) excited by 488 nm laser which is normalized with the first fluorescence intensity($F_0$) in the specific cell region. Each single lysosome boundary was drawn and analyzed the movement of $Ca^{2+}$ concentration during the experiments.

### TRPML activity measurement via GCaMP6s fused TRPML

GCaMP6s-TRPML1 and GCaMP6s-TRPML2 plasmids were transfected into Ramos or HeLa cells expressing CD20. After 48 h, fluorescence changes were monitored using confocal microscopy (LSM 710, Zeiss) in a 1.5 mM $Ca^{2+}$ regular solution containing 150 mM NaCl, 5 mM KCl, 1 mM $MgCl_2$, 10 mM glucose, 10 mM HEPES. Cells were treated with mAbs (10 μg/ml) for 5 min then treated ML-SA1 (20 μM). Fluorescence changes ($\Delta F/F_0$) were analysed in defined regions of interest.

### Quantification of endocytosis of pHAb labelled-antibody

pHAb-labeled antibodies were prepared, purified, and quantified using Nanodrop. Raji cells ($2 \times 10^5$) were treated with antibody-pHAb (10 μg/ml, #G9845, Promega) for the indicated times, and internalization was analyzed by FACS. Internalization rate was calculated as following. The values taken at each time point were normalized by $F_0$, and the difference in binding affinity of RTX and OBI and the DAR.

$$\frac{F_t - F_0}{F_t} \times bindingaffinityratio \times dyetoantibodyratio(DAR)$$

### Electron microscopy with immune-gold labelled antibodies

RTX and OBI (0.25 mg/ml) were conjugated to gold nanoparticles (Gold Nanoparticles Kit, Innova Biosciences, UK), fixed, and post-fixed with osmium tetroxide. Ramos cells ($5 \times 10^6$) were processed for EM imaging, including ethanol dehydration, embedding, and ultrathin sectioning. Samples were imaged using EM microscopy.

### EGFP-NT-lysenin staining for sphingomyelin localization along with OBI or RTX

Recombinant EGFP-NT-lysenin (pET28/His6-EGFP-NT-Lysenin; RDB13498, RIKEN) was used as a sphingomyelin probe in Raji cells. Cells were pre-incubated with 10 μg/ml of purified EGFP-lysenin for 30 min, followed by treatment with Dylight-labeled antibodies (10 μg/ml each) at either 4 °C or 37 °C for 30 min. After incubation, cells were washed with PBS and fixed in 4% paraformaldehyde. Confocal images were acquired using a Zeiss LSM 710 confocal microscope (Carl Zeiss).

### Statistical analysis

For comparisons between two groups, the Mann–Whitney U test was used. For multiple-group comparisons, one-way ANOVA was performed followed by Dunnett's multiple-comparisons test when comparing each condition to a single control, or Tukey's multiple-comparisons test when comparing all pairs. Statistical significance is indicated as $p < 0.05$, $p < 0.01$, $p < 0.001$, $p < 0.0001$.

## Results

### TRPML inhibition enhances OBI-induced LMP and DCD

We first examined whether lysosomal membrane tension regulates OBI-induced cytotoxicity. Altering osmotic conditions revealed that hypotonic stress, which increases lysosomal swelling[15,16], significantly enhanced both LMP and DCD, whereas hypertonic stress suppressed them (Fig. 1a). RT-PCR profiling confirmed TRPML2 as the most abundantly expressed isoform in Raji and Ramos cells (Supplementary Fig. 1). Pharmacological inhibition of TRPMLs with (1R,2R)-ML-SI3 further enhanced OBI-induced LMP and was associated with a modest but statistically significant increase in DCD (Fig. 1b,c). PIKfyve inhibition with Apilimod further enhanced OBI-induced responses, consistent with prior reports[22,25], but this effect was not observed when TRPMLs were inhibited (Fig. 1b). TRPMLs inhibitors, (1R, 2R)-ML-SI3, had stronger effects than TRPML1 inhibitors such as EDME (2-(2,5-dimethyl-1H-pyrrol-1-yl)-*N*-(2-methoxyethyl)-2-oxoacetamide) (Supplementary Fig. 2). Consistent with this pharmacological evidence, siRNA-mediated knockdown of TRPML2 significantly enhanced OBI-induced cytotoxicity (Fig. 1d,e; Supplementary Fig. 3). Furthermore, CRISPRi-mediated knockdown experiments confirmed that TRPML2 suppression produced the highest levels of OBI-induced cell death compared to TRPML1 knockdown or mock cells (Supplementary Fig. 4). Morphological assays showed lysosomal enlargement under hypotonic stress, and similar enlargement was observed upon TRPML inhibition (Fig. 1f) and increased cathepsin release when combined with OBI (Fig. 1g,h). Together, these results establish TRPML2 as a critical regulator of lysosomal stability during OBI-induced DCD.

### OBI suppresses TRPML $Ca^{2+}$ channel activity

To determine whether OBI directly interferes with TRPML channel function, we performed a series of assays using the TRPMLs-specific agonist ML-SA1 stimulation, reporter-based imaging methods such as Fluo-4, Oregon-BAPTA, and TRPML2–GCaMP6s. First, cytosolic $Ca^{2+}$ dynamics were measured in Ramos cells using Fluo-4. In control cells, ML-SA1 induced a robust cytosolic $Ca^{2+}$ rise, but this response was completely abolished in OBI-treated cells (Fig. 2a,b). Lysosomal $Ca^{2+}$ imaging with Oregon-BAPTA demonstrated that OBI markedly suppressed ML-SA1–induced $Ca^{2+}$ release while leaving basal lysosomal $Ca^{2+}$ levels unchanged (Fig. 2c–e). These data suggested that OBI blocks TRPML-dependent $Ca^{2+}$ flux. Next, we directly visualized TRPML2 activity using a TRPML2–GCaMP6s (a genetically encoded $Ca^{2+}$ indicator consisting of GFP fused to calmodulin and an M13 peptide, whose fluorescence increases upon $Ca^{2+}$ binding) fusion construct localized to lysosomes (Supplementary Fig. 5). In untreated cells, ML-SA1 stimulation produced strong fluorescence increases, confirming TRPML2 activation. In contrast, OBI-treated cells failed to show any increase (Fig. 2f,g). Importantly, cells expressing constitutively active TRPML2$^{Va}$ mutants (A396P; alanine-to-proline substitution)[26] retained $Ca^{2+}$ responses despite OBI treatment (Fig. 2h,i), confirming the specificity of OBI-mediated inhibition. Parallel assays with TRPML1–GCaMP6s also revealed inhibition (Supplementary Fig. 6). The suppression was dose- and time-dependent, with complete inhibition achieved within 5 min at 3 μg/ml (Fig. 3j,k). Lysotracker staining confirmed intact lysosomes during this early period (Supplementary Fig. 7), indicating that TRPML2 inhibition precedes overt LMP.

Taken together, the ML-SA1 stimulation assays and live-cell TRPML2–GCaMP6s reporter imaging consistently demonstrate that OBI rapidly and specifically inhibits TRPML2 channel activity. This inhibition represents an early and essential event that sensitizes lysosomes to permeabilization and drives OBI-induced direct cell death.

### Filipin-sensitive trafficking is associated with OBI-induced TRPML2 inhibition

Immunogold TEM provided a qualitative snapshot of antibody distribution and membrane ultrastructure, showing that RTX was predominantly associated with the plasma membrane (often at thickened/raft-like regions), whereas OBI was readily detected in intracellular vesicular structures at early time points (Fig. 3a,b). However, as TEM is a qualitative imaging method, it does not provide a quantitative readout of antibody internalization dynamics. To quantitatively monitor antibody trafficking to acidic compartments, we conjugated pHAb dyes to RTX and OBI, which increase fluorescence upon exposure to acidic environments (Supplementary Fig. 8). pHAb fluorescence measurements revealed that OBI accumulated in acidic compartments faster than RTX (Fig. 3c). This result demonstrates that OBI's internalization rate is more than twice as fast as RTX, with a clear and rapid accumulation in acidic vesicles. Furthermore, comparable binding of pHAb-labeled antibodies to Raji cells was confirmed by flow cytometry (Supplementary Fig. 8c).

To probe the uptake/trafficking step linked to TRPML2 inhibition, we monitored TRPML2 activity using the GCaMP6s-TRPML2 reporter while pharmacologically perturbing endocytic processes (Fig. 3d–i; Supplementary Fig. 9). Under these conditions, filipin prevented OBI-mediated TRPML2 inhibition, whereas dynasore and

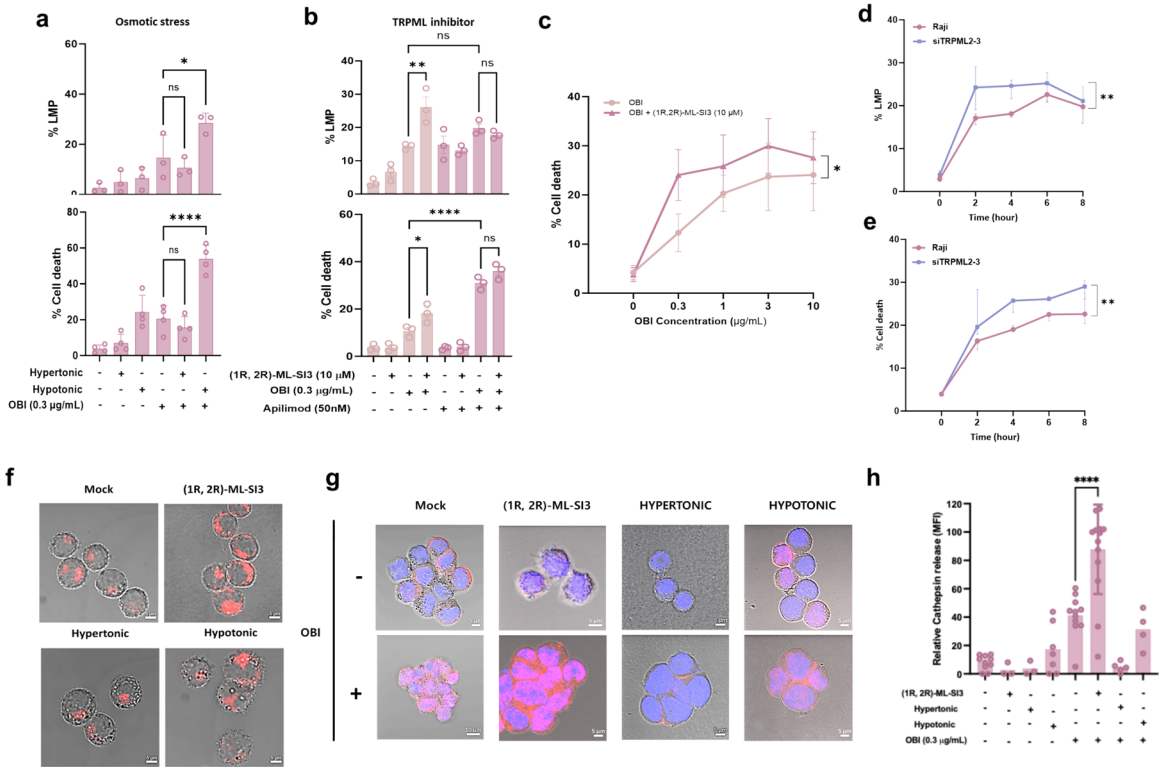


**Fig. 1**. Lysosomal stress and TRPML inhibition enhance obinutuzumab-mediated direct cell death. (**a**) LMP and DCD were measured in Raji cells treated with hypertonic medium (200 mM sucrose) or hypotonic medium (60% distilled water in complete culture medium) for 2 h in the presence of OBI (Hereafter, the concentration of OBI is 10 μg/ml unless otherwise stated). LMP and DCD were evaluated by LysoTracker Green and propidium iodide (PI) staining. One-way ANOVA with Dunnett's multiple-comparisons test (vs. control). (**b**) OBI-induced LMP and DCD were assessed in Raji cells co-incubated with increasing concentrations of the TRPML inhibitor (1R,2R)-ML-SI3 (10 μM). In parallel, cells pretreated overnight with the PIKfyve inhibitor Apilimod (50 nM) showed enhanced OBI responses, but this effect was abolished when TRPMLs were simultaneously inhibited. One-way ANOVA with Dunnett's multiple-comparisons test (vs. control). (**c**) Dose-dependent enhancement of OBI-induced DCD was observed following 2-h co-incubation with a fixed concentration of the (1R,2R)-ML-SI3 (10 μM, over 2 h incubation, this (1R,2R)-ML-SI3 treatment condition was used unless otherwise stated). (**d**,**e**) Time-dependent enhancement of OBI-induced LMP (**d**) and DCD (**e**) were assessed in TRPMLs-targeting siRNA cell lines. (**f**) Lysosome enlargement and fluorescence intensity were indicated by LT Deep Red staining, then imaged by confocal microscopy. (1R, 2R)-ML-SI3, hypertonic, and hypotonic medium were incubated 2 h. Scale bars in all images represent 5 μM. (**g**,**h**) Quantification of cathepsin B release induced by OBI and (1R,2R)-ML-SI3 treatment. (**g**) Raji cells were treated with (1R,2R)-ML-SI3, hypertonic medium (200 mM sucrose), or hypotonic medium (60% distilled water in complete medium) for 2 h, and with OBI for 4 h. Cathepsin B releases were visualized by confocal microscopy by immunostaining. (**h**) The summary of the release data shows significant cathepsin B secretion in response to OBI treatment, which was further modulated by (1R,2R)-ML-SI3 and osmotic stress conditions. Data are presented as mean ± SEM. *$p < 0.05$, ***$p < 0.001$ compared to obi-treated group.

pitstop2 did not, indicating involvement of a filipin-sensitive (cholesterol-dependent) step upstream of TRPML2 inhibition. However, in the LMP and DCD assays, filipin produced only modest/partial attenuation of OBI-induced phenotypes, suggesting that additional factors beyond TRPML2 inhibition contribute to downstream lysosomal membrane permeabilization and cell death. Consistent with this, conditions that preserved TRPML2 activity were associated with reduced OBI-induced LMP and direct cell death (Fig. 3j,k). Filipin-sensitive inhibition of OBI internalization shows that the TRPML2 suppression by OBI is dependent on a filipin-sensitive step that blocks OBI internalization. (Fig. 3l). These findings implicate a filipin-sensitive, cholesterol-dependent uptake/trafficking step in OBI-induced TRPML2 inhibition.

## Sphingomyelin is functionally linked to OBI-induced TRPML2 inhibition

Because sphingomyelin (SM) has been reported to inhibit TRPML1-3 and has been proposed as a potential regulator of other TRPML channels, we tested whether SM contributes to OBI-induced TRPML2 dysfunction. SMase treatment, which depletes cell-surface/accessible SM, restored ML-SA1–evoked TRPML2 activity in a dose-dependent manner (Fig. 4a,b). In contrast, heat-inactivated SMase failed to rescue TRPML2 activity,

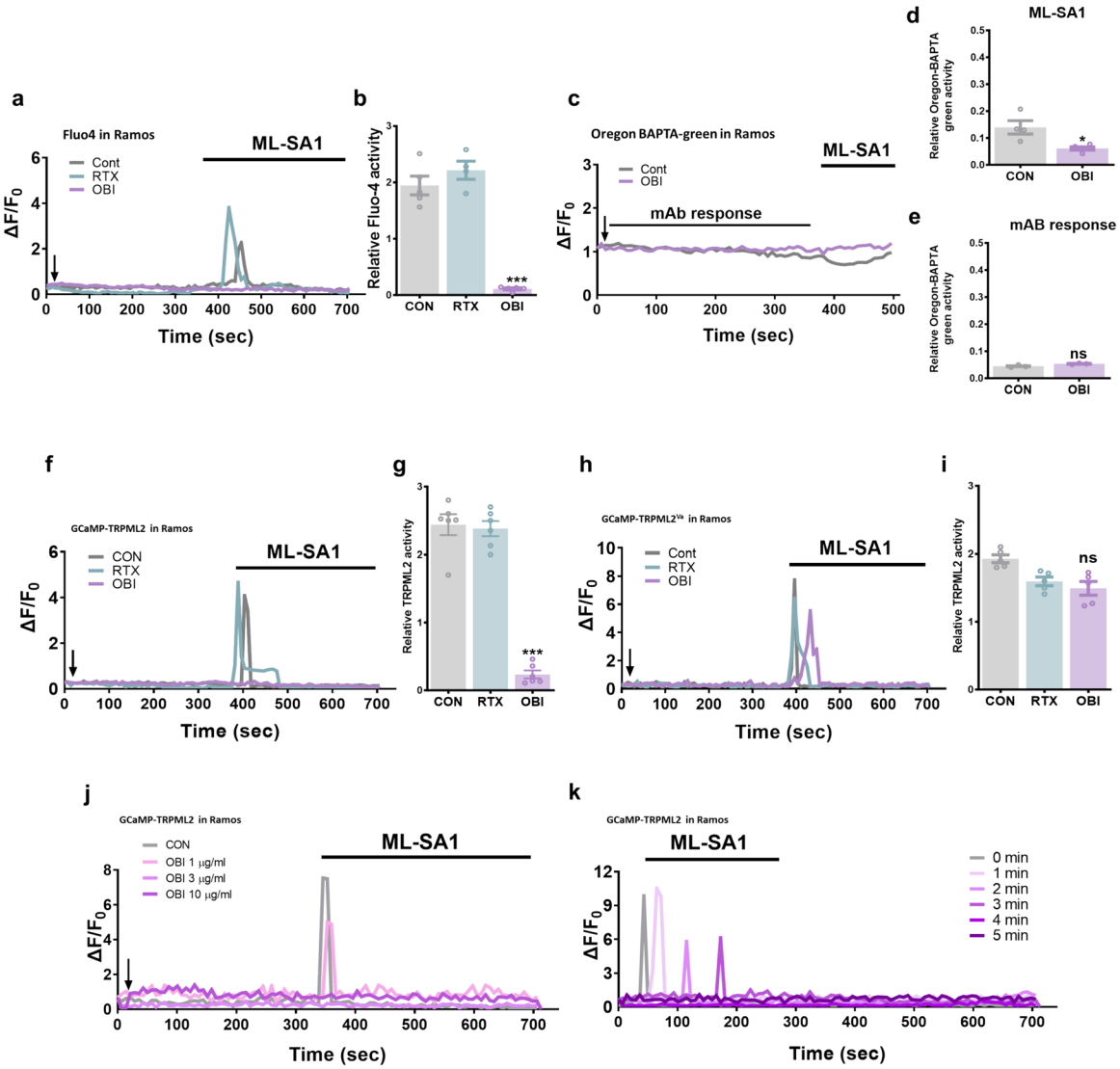


**Fig. 2**. Obinutuzumab inhibits TRPML2-Mediated Lysosomal $Ca^{2+}$ Release. (**a**,**b**) To measure time dependent TRPML2 inhibition, ML-SA1 was treated at indicated time point after 10 μg/ml OBI treatment. Average cytosolic $Ca^{2+}$ increases were observed in control, RTX (10 μg/ml), and OBI (10 μg/ml) treated Ramos cells upon ML-SA1 treatment using Fluo-4 $Ca^{2+}$ dye. (**c**) Time-course traces of lysosomal $Ca^{2+}$-dependent fluorescence in Ramos cells loaded with Oregon Green BAPTA–dextran. After pretreatment with mock (vehicle) or OBI (10 μg/ml), cells were stimulated with ML-SA1 during the time window indicated. (**d**) Quantification of the mean Oregon Green BAPTA–dextran fluorescence averaged over the ML-SA1 stimulation window indicated in (**c**), comparing mock- vs OBI-pretreated cells. (**e**) Quantification of the mean Oregon Green BAPTA–dextran fluorescence averaged over the antibody-treatment window (indicated in the trace), comparing mock (vehicle) and OBI conditions. Data are presented as mean ± SEM. *$p < 0.05$, ***$p < 0.001$ vs the mock (vehicle) control. (**e**) Average fluorescence changes of Oregon Green BAPTA-dextran under mock conditions and during OBI treatment. (**f**,**i**) Evaluation of OBI's effect on TRPML2 activity in Ramos cells using fluorescence changes of TRPML2-GCaMP6s (**f**,**g**) and GCaMP6s-TRPML2$^{Va}$ (**h**,**i**). Following antibody treatment, fluorescence trends of GCaMP were tracked upon administration of 20 μM ML-SA1 at indicated points. Fluorescence changes in GCaMP6s-TRPML2 and GCaMP6s-TRPML2$^{Va}$ expressing cells were assessed upon ML-SA1 induction compared to control, RTX, and OBI treatment. (**j**,**k**) The traces of GCaMP6s-TRPML2 fluorescence showing OBI-time (10 μg/ml) (**j**) and -dose (**k**) dependent, achieving full inhibition at 3 μg within 5 min. One-way ANOVA with Dunnett's multiple-comparisons test (vs. control) used in (**b**,**g**,**i**). Unpaired two-tailed Student's t-test used in (**d**,**e**). Data are presented as mean ± SEM. *$p < 0.05$, ***$p < 0.001$ compared to control group. Data are presented as mean ± SEM. *$p < 0.05$, ***$p < 0.001$ compared to control group.

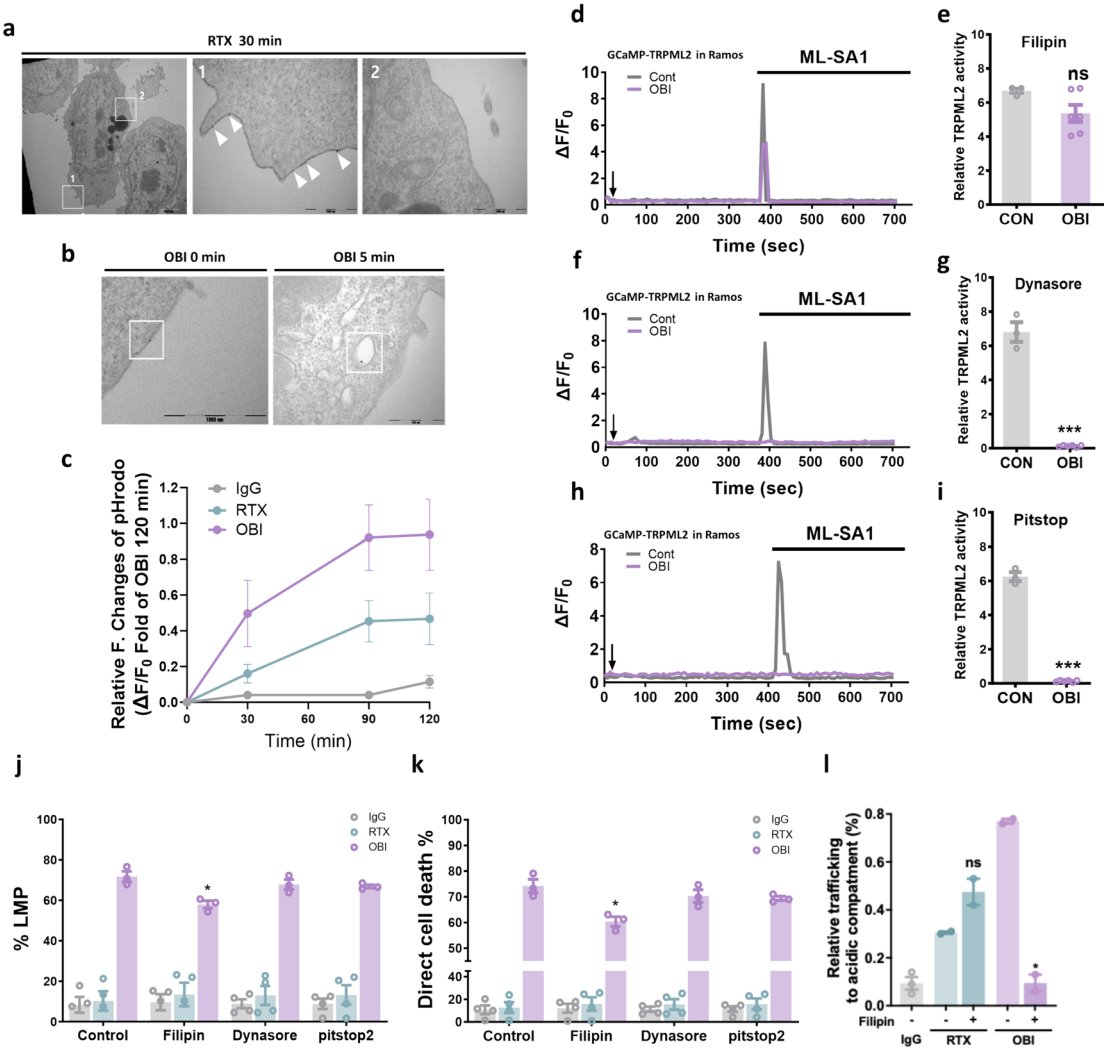


**Fig. 3**. TRPML2 inhibition by OBI is mediated through caveolin-dependent endocytosis. (**a**,**b**) Transmission electron microscopy with 10 nm gold-labeled antibodies was used to assess subcellular localization. RTX (10 µg/ml) (**a**) was mainly retained on the plasma membrane after 30 min at 37 °C, with gold particles clustered at thicker regions (arrowheads) and absent from thinner membrane areas. OBI (10 µg/ml) (**b**), in contrast, was initially surface bound at 0 min but appeared within intracellular vesicles after 5 min of incubation at 37 °C. Scale bars: 1000 nm (overview), 500 nm (magnified views). (**c**) Relative mean fluorescence of pHAb-labeled antibodies over time, with fluorescence change value (ΔF) at each time point, expressed as a ratio to the initial fluorescence value ($F_0$) and the value at 120 min ($F_{120}$) of OBI (10 µg/ml) incubation. (**d–i**) Filipin-sensitive TRPML2 inhibition by OBI measured by changes in GCaMP6s-TRPML2 fluorescence in Ramos cells pre-treated with endocytosis inhibitors including 80 µM Filipin (**d**,**e**), 10 µM Dynasore (**f**,**g**), and 2.5 µM Pitstop (**h**,**i**) for 30 min at 37 °C. Unpaired two-tailed Student's t-test used in (**e**,**g**,**i**). (**j**,**k**) Before antibody treatment (10 µg/ml, each), Raji cells were pre-incubated with endocytosis inhibitors (Filipin, Dynasore, and Pitstop2; pre-treated for 30 min at 37 °C). LMP (**j**) and DCD (**k**) were assessed by Lysotracker Red and Calcein fluorescence, respectively. One-way ANOVA with Dunnett's multiple-comparisons test (vs. control) used in (**j**,**k**). (**l**) Filipin (80 µM) effect on internalization of 10 µg/ml each antibody. Data are presented as mean ± SEM. *$p < 0.05$, **$p < 0.01$ vs. control.

indicating that enzymatic SM hydrolysis is required (Fig. 4c,d). Effective depletion of accessible SM by SMase was confirmed by loss of EGFP-lysenin binding[27] (Supplementary Fig. 10).

To assess whether OBI trafficking is associated with SM-positive compartments, we used recombinant EGFP-lysenin, an SM-binding probe, to lable plasma membrane-localized SM with extracellular treatment. This probe redistributes from diffuse cytosolic fluorescence to punctate membrane-associated signals upon binding accessible SM on intracellular membrane structures. Confocal imaging revealed increased EGFP-NT-lysenin puncta associated with OBI-positive acidic compartments compared to RTX (Fig. 4e), to punctate membrane-associated signals upon binding accessible SM on intracellular membrane structures. Confocal imaging showed increased EGFP-lysenin puncta associated with OBI-positive acidic compartments compared with RTX (Fig. 4e). Functionally, SMase pretreatment attenuated OBI-induced LMP and direct cell death (Fig. 4f,g),

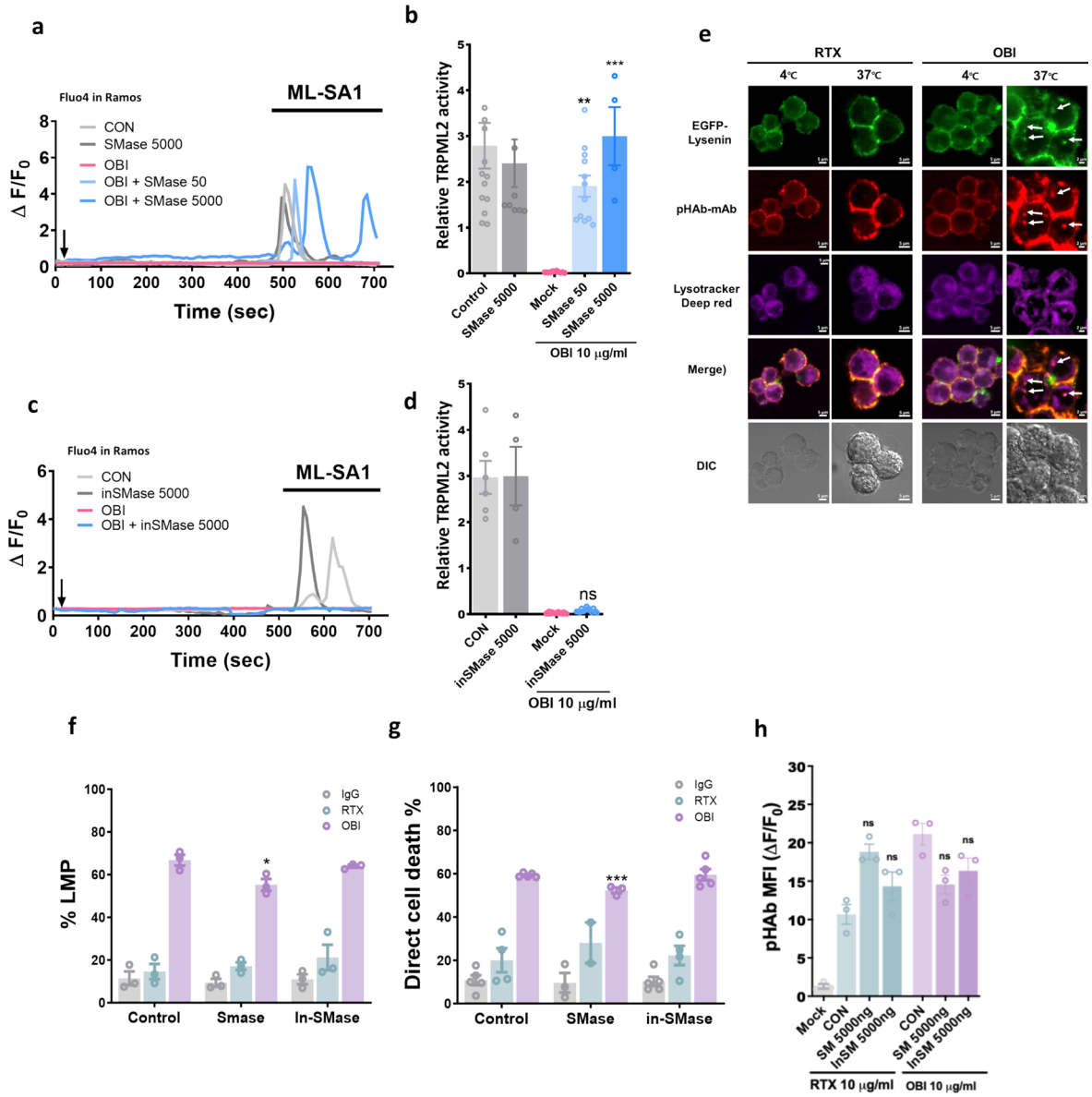


**Fig. 4**. Sphingomyelinase (SMase) rescues OBI-associated TRPML2 dysfunction and attenuates downstream LMP and direct cell death. (**a**–**d**) Mean fluorescence traces of the GCaMP6s–TRPML2 reporter in Ramos cells. Cells were treated with OBI (10 μg/ml) at time 0, followed by stimulation with ML-SA1 at the indicated time point. Cells were pretreated with active bacterial sphingomyelinase (SMase; 50 ng or 5000 ng) (**a**,**b**) or heat-inactivated SMase (5000 ng) (**c**,**d**) prior to OBI exposure. (**b**,**d**) Quantification of ML-SA1-evoked TRPML2-mediated $Ca^{2+}$ release (average fluorescence change during the ML-SA1 period) under the indicated conditions. Data are presented as mean ± SEM. Unpaired two-tailed Student's t-test. ***$p < 0.001$ vs. Mock. (**e**) Confocal images of recombinant EGFP-NT-lysenin-stained Raji cells (green) incubated with pHAb-labeled RTX or OBI (red), each at 10 μg/ml. Lysotracker was used to identify lysosomes, where OBI and EGFP-NT-lysenin puncta are located. Arrows indicate representative regions where the EGFP-NT-lysenin signal co-localizes with OBI in the lysosome. (**f**,**g**) LMP (**f**) and direct cell death (DCD) (**g**) assays in Raji cells pretreated with active or heat-inactivated SMase. Cells were pre-incubated with SMase at 37 °C, 5% $CO_2$ for 30 min, then treated with RTX or OBI (10 μg/ml each). Live cells were stained with LysoTracker and calcein-AM and analyzed by flow cytometry. (**h**) Quantitative analysis of pHAb-labeled OBI internalization following SMase treatment. Data are presented as mean ± SEM. One-way ANOVA with Dunnett's multiple-comparisons test (vs. control). ***$p < 0.001$ vs. control.

supporting a model in which SM-dependent TRPML2 inhibition sensitizes lysosomes to OBI-induced stress, lowering the threshold for lysosomal destabilization. Notably, SMase treatment did not affect OBI internalization (Fig. 4h indicating that the observed effects on TRPML2 inhibition and downstream lysosomal dysfunction are not dependent on changes in OBI internalization. This suggests that OBI internalization occurs independently

of SMase-induced alterations in cell-surface sphingomyelin, further implicating other lipid-trafficking and/or endocytic pathways in OBI's action.

## Discussion

This study delineates a lipid–ion channel axis associated with how obinutuzumab (OBI) induces direct cell death (DCD) in B-cell lymphoma through lysosomal destabilization. We show that OBI is rapidly internalized into acidic compartments and that this trafficking is linked to sphingomyelin (SM)-dependent events accompanied by suppression of TRPML2-mediated lysosomal $Ca^{2+}$ release. Together, these findings provide mechanistic context connecting antibody trafficking with lysosomal membrane permeabilization (LMP) and DCD.

Several aspects of these findings merit further consideration. First, functional imaging and genetic perturbation support TRPML2 as a key lysosomal channel modulated in the context of OBI treatment, and TRPML2 inhibition appears to occur early in the process. Importantly, however, TRPML inhibition alone under basal conditions is not sufficient to robustly induce LMP, suggesting that TRPML2 suppression is more likely to act as a sensitizing step that lowers the threshold for lysosomal destabilization rather than serving as the sole trigger. Dampening TRPML2-mediated $Ca^{2+}$ release is expected to impair endo-lysosomal trafficking and stress adaptation, thereby predisposing lysosomes to permeabilization and downstream lysosome-dependent cell death (LDD) in stressed cells[28].

Second, OBI's trafficking pattern differs from that of rituximab, highlighting how variations in antibody internalization pathways can translate into distinct cytotoxic outcomes. Understanding how Fc engineering or glycosylation influence such trafficking properties may provide useful design principles for next-generation therapeutic antibodies.

Third, sphingolipid biology emerges as an important determinant of this phenotype. The observation that SMase treatment rescues TRPML2 activity and attenuates downstream LMP/DCD supports involvement of an SM-dependent step upstream of TRPML2 inhibition. Consistent with this interpretation, SMase did not measurably change OBI internalization (Fig. 4h). This supports a model in which SM primarily acts on downstream lipid/ion-channel regulation rather than antibody uptake and suggests additional trafficking or endocytic pathways linking OBI trafficking to TRPML2 inhibition. Our imaging with EGFP-lysenin is consistent with changes in SM-associated signals in OBI-positive acidic compartments; however, EGFP-lysenin reports binding to accessible SM on membrane structures and does not directly quantify total lysosomal SM pools or specific sphingolipid species. Thus, while our data support an SM-linked mechanism, additional lipidomic approaches will be required to define how SM distribution and composition change at the endolysosomal membrane during OBI trafficking. Furthermore, it remains uncertain whether SM itself is sufficient to promote LMP through TRPML2 inhibition, or whether downstream metabolites such as sphingosine[29] contribute to membrane fragility and lysosomal destabilization. Because sphingolipid species can exert diverse and sometimes opposing functions, and multiple strategies to dissect these pathways have been reported31, further studies will be needed to establish the relative contributions of SM and its metabolites in this setting.

From a translational perspective, these findings extend our understanding of why OBI can display superior cytotoxicity compared to rituximab. Modulating trafficking-linked sphingolipid signals or TRPML2 activity may provide a route to tune lysosomal vulnerability and thereby amplify antibody-driven DCD, potentially enhancing immunogenic effects through the release of damage-associated molecular patterns (DAMPs). It will be important to determine whether similar SM–TRPML2 dynamics operate in vivo and in patient samples, and whether pharmacologic or genetic interventions targeting this axis improve therapeutic outcomes.

In summary, OBI engages an SM-dependent trafficking step associated with suppression of TRPML2-mediated lysosomal $Ca^{2+}$ release, which sensitizes lysosomes and promotes LMP and DCD in the context of OBI-induced stress. These insights advance mechanistic understanding of antibody-induced cell death and highlight lipid trafficking and lysosomal ion-channel regulation as potential targets for future therapeutic antibody development.

## Data availability

The datasets generated and analyzed during the current study are available from the corresponding author upon reasonable request. All raw data supporting the findings of this study are available from the corresponding author upon reasonable request. No human-identifiable data are included.

Received: 14 October 2025; Accepted: 28 January 2026
Published online: 03 February 2026

## References

1. Niederfellner, G. et al. Epitope characterization and crystal structure of GA101 provide insights into the molecular basis for type I/II distinction of CD20 antibodies. *Blood* **118**, 358–367. https://doi.org/10.1182/blood-2010-09-305847 (2011).
2. Sean, H. L. et al. Anti-CD20 monoclonal antibodies: Historical and future perspectives. *Haematologica* **95**, 135–143. https://doi.org/10.3324/haematol.2008.001628 (2010).
3. Herter, S. et al. Preclinical activity of the type II CD20 antibody GA101 (obinutuzumab) compared with rituximab and ofatumumab in vitro and in xenograft models. *Mol. Cancer Ther.* **12**, 2031–2042. https://doi.org/10.1158/1535-7163.mct-12-1182 (2013).
4. Klein, C. et al. Epitope interactions of monoclonal antibodies targeting CD20 and their relationship to functional properties. *MAbs* **5**, 22–33. https://doi.org/10.4161/mabs.22771 (2013).
5. Marcus, R. et al. Obinutuzumab for the first-line treatment of follicular lymphoma. *N. Engl. J. Med.* **377**, 1331–1344. https://doi.org/10.1056/NEJMoa1614598 (2017).
6. Herter, S. et al. GA101 P329GLALA, a variant of obinutuzumab with abolished ADCC, ADCP and CDC function but retained cell death induction, is as efficient as rituximab in B-cell depletion and antitumor activity. *Haematologica* **103**, e78–e81. https://doi.org/10.3324/haematol.2017.178996 (2018).

7. Tobinai, K., Klein, C., Oya, N. & Fingerle-Rowson, G. A review of obinutuzumab (GA101), a novel type II anti-CD20 monoclonal antibody, for the treatment of patients with B-cell malignancies. *Adv. Ther.* **34**, 324–356 (2017).
8. Alduaij, W. et al. Novel type II anti-CD20 monoclonal antibody (GA101) evokes homotypic adhesion and actin-dependent, lysosome-mediated cell death in B-cell malignancies. *Blood* **117**, 4519–4529. https://doi.org/10.1182/blood-2010-07-296913 (2011).
9. Zhang, F. et al. Combating rituximab resistance by inducing ceramide/lysosome-involved cell death through initiation of CD20-TNFR1 co-localization. *Oncoimmunology* **5**, e1143995. https://doi.org/10.1080/2162402x.2016.1143995 (2016).
10. Xu, H. & Ren, D. Lysosomal physiology. *Annu. Rev. Physiol.* **77**, 57–80. https://doi.org/10.1146/annurev-physiol-021014-071649 (2015).
11. Aits, S. et al. Sensitive detection of lysosomal membrane permeabilization by lysosomal galectin puncta assay. *Autophagy* **11**, 1408–1424 (2015).
12. Blomgran, R., Zheng, L. & Stendahl, O. Cathepsin-cleaved Bid promotes apoptosis in human neutrophils via oxidative stress-induced lysosomal membrane permeabilization. *J. Leukoc. Biol.* **81**, 1213–1223. https://doi.org/10.1189/jlb.0506359 (2007).
13. Aits, S. & Jäättelä, M. Lysosomal cell death at a glance. *J. Cell Sci.* **126**, 1905–1912. https://doi.org/10.1242/jcs.091181 (2013).
14. Boya, P. & Kroemer, G. Lysosomal membrane permeabilization in cell death. *Oncogene* **27**, 6434–6451. https://doi.org/10.1038/onc.2008.310 (2008).
15. Hu, M., Zhou, N., Cai, W. & Xu, H. Lysosomal solute and water transport. *J. Cell Biol.* **221**, e202109133 (2022).
16. Li, P. et al. LRRC8 family proteins within lysosomes regulate cellular osmoregulation and enhance cell survival to multiple physiological stresses. *Proc. Natl. Acad. Sci.* **117**, 29155–29165 (2020).
17. Colletti, G. A. et al. Loss of lysosomal ion channel transient receptor potential channel mucolipin-1 (TRPML1) leads to cathepsin B-dependent apoptosis. *J. Biol. Chem.* **287**, 8082–8091 (2012).
18. Scotto Rosato, A. et al. TRPML1 links lysosomal calcium to autophagosome biogenesis through the activation of the CaMKKβ/VPS34 pathway. *Nat. Commun.* **10**, 5630 (2019).
19. Cao, Q., Yang, Y., Zhong, X. Z. & Dong, X.-P. The lysosomal Ca2+ release channel TRPML1 regulates lysosome size by activating calmodulin. *J. Biol. Chem.* **292**, 8424–8435 (2017).
20. Schmiege, P., Fine, M., Blobel, G. & Li, X. Human TRPML1 channel structures in open and closed conformations. *Nature* **550**, 366–370 (2017).
21. Chen, C.-C. et al. TRPML2 is an osmo/mechanosensitive cation channel in endolysosomal organelles. *Sci. Adv.* **6**, eabb5064 (2020).
22. Choy, C. H. et al. Lysosome enlargement during inhibition of the lipid kinase PIKfyve proceeds through lysosome coalescence. *J. Cell Sci.* **131**, jcs213587 (2018).
23. Shen, D. et al. Lipid storage disorders block lysosomal trafficking by inhibiting a TRP channel and lysosomal calcium release. *Nat. Commun.* **3**, 731 (2012).
24. Gabandé-Rodríguez, E., Boya, P., Labrador, V., Dotti, C. & Ledesma, M. High sphingomyelin levels induce lysosomal damage and autophagy dysfunction in Niemann Pick disease type A. *Cell Death Differ.* **21**, 864–875 (2014).
25. Kim, Y., Oh, J., Kim, J. R., Lee, D. & Kim, J. Y. CRISPRi screening identifies PIKfyve as a co-therapeutic target for obinutuzumab. *Clin. Transl. Med.* **15**, e70333 (2025).
26. Xu, H., Delling, M., Li, L., Dong, X. & Clapham, D. E. Activating mutation in a mucolipin transient receptor potential channel leads to melanocyte loss in varitint-waddler mice. *Proc. Natl. Acad. Sci. U. S. A.* **104**, 18321–18326. https://doi.org/10.1073/pnas.0709096104 (2007).
27. Shogomori, H. & Kobayashi, T. Lysenin: A sphingomyelin specific pore-forming toxin. *Biochim. Biophys. Acta BBA Gen. Subj.* **1780**, 612–618. https://doi.org/10.1016/j.bbagen.2007.09.001 (2008).
28. Morelli, M. B. *et al.* Overexpression of transient receptor potential mucolipin-2 ion channels in gliomas: role in tumor growth and progression. *Oncotarget.* **7** (2016).
29. Jiménez-Rojo, N. et al. Membrane permeabilization induced by sphingosine: Effect of negatively charged lipids. *Biophys. J .* **106**, 2577–2584. https://doi.org/10.1016/j.bpj.2014.04.038 (2014).


## Acknowledgements

The authors are deeply grateful to Professor Haoxing Xu (Department of Molecular, Cellular, and Developmental Biology, University of Michigan), for kindly providing the GCaMP-TRPML1 clone.

## Author contributions

J.O. performed both LMP and DCD-related experiments with various lysosome-regulating drugs. J.O. and C.L. performed imaging analysis with confocal microscopy. N.J. performed most of the TRPML2-GCaMP experiment. S.K. performed the endocytosis of OBI. C.L. and H.B. helped Obinutuzumab production and DCD assay. D.L. supervised technical processes. J.Y.K. organized and supervised the whole project. J.O. and J.Y.K. wrote the manuscript.

## Funding

This work was supported by grants from the National Research Foundation of Korea, Project Nos. NRF-2019R1A2C1086348 and RS-2023-00220853 to J.Y.K. The funders had no role in study design, data collection and analysis, decision to publish, or preparation of the manuscript.

## Competing interests

The authors declare no competing interests.

## Consent to participate

Patient-derived PBMC samples were isolated with approval of Yonsei University Institutional Review Committee after obtaining informed consent, under IRP procedure (#4-2022-0471).

## Additional information

**Supplementary Information** The online version contains supplementary material available at https://doi.org/10.1038/s41598-026-38087-5.

**Correspondence** and requests for materials should be addressed to J.Y.K.

**Reprints and permissions information** is available at www.nature.com/reprints.